

Article

Optimization of Plasmonic Copper Content at Copper-Modified Strontium Titanate (Cu-SrTiO₃): Synthesis, Characterization, Photocatalytic Activity

Áron Ágoston ¹, Ádám Balog ², Šarūnas Narbutas ³, Imre Dékány ^{1,*} and László Janovák ^{1,*} 

¹ Department of Physical Chemistry and Materials Sciences, University of Szeged, Rerrich B. Sqr.1, H-6720 Szeged, Hungary

² Department of Physical Chemistry and Materials Science, Interdisciplinary Excellence Centre, University of Szeged, Rerrich Square 1, H-6720 Szeged, Hungary

³ UAB “Kai reikia” Director, Savanorių pr. 303, LT-45301 Kaunas, Lithuania

* Correspondence: i.dekany@chem.u-szeged.hu (I.D.); janovakl@chem.u-szeged.hu (L.J.); Tel.: +36-62-544-210 (I.D. & L.J.)

Abstract: Catalyst development still has a major impact on science today, as we can use catalysts to break down certain pollutants in an energy-efficient way. There is no comprehensive literature on the development of SrTiO₃-based photocatalysts, so study in this area is justified. Related to this topic, here we report the facile preparation of surface-modified SrTiO₃ photocatalyst, performed by plasmonic copper deposition. In the case of the copper-modified samples (0.25–3 wt.% Cu content), the photooxidation of phenol, as model contaminant, was almost 4–5 times higher than the bare SrTiO₃. However, the photocatalytic activity was not linearly related to copper content, since the highest photoactivity was achieved at 1 wt.% copper content. The reason for the better activity was the plasmonic effect of copper, which increases the recombination time of charge separation on the catalyst surface. During slower recombination, more water is oxidized to hydroxyl radicals, which can lead to faster degradation of phenol.

Keywords: strontium-titanate; copper surface deposition; plasmonic effect; copper content optimization; hydroxyl radical; recombination time



Citation: Ágoston, Á.; Balog, Á.; Narbutas, Š.; Dékány, I.; Janovák, L. Optimization of Plasmonic Copper Content at Copper-Modified Strontium Titanate (Cu-SrTiO₃): Synthesis, Characterization, Photocatalytic Activity. *Catalysts* **2022**, *12*, 1041. <https://doi.org/10.3390/catal12091041>

Academic Editor: Simonetta Palmas

Received: 29 July 2022

Accepted: 12 September 2022

Published: 13 September 2022

Publisher's Note: MDPI stays neutral with regard to jurisdictional claims in published maps and institutional affiliations.



Copyright: © 2022 by the authors. Licensee MDPI, Basel, Switzerland. This article is an open access article distributed under the terms and conditions of the Creative Commons Attribution (CC BY) license (<https://creativecommons.org/licenses/by/4.0/>).

1. Introduction

Photocatalyst development is a supported and intensively researched field of chemistry, even nowadays. These catalysts are suitable for water purification, air cleaning, antimicrobial treatment, and many other beneficial applications [1–6]. The photocatalysts are often metal oxide-based materials, metal oxide semiconductors or composites, and the most popular members are based on titanium, e.g., TiO₂, metal or nonmetal modified TiO₂, MeTiO₃ (Me: alkaline metal, alkaline earth metal, transition metal) [7,8]. Nowadays, SrTiO₃ is an intensively researched photocatalyst because it has many benefits, like inertness, nontoxicity, low cost and high stability. SrTiO₃ is a typical semiconductor photocatalyst oxide, which has relatively high photocatalytic activity in the UV region. The modification of SrTiO₃ usually results in increased photocatalytic activity [9–11].

Heterogeneous photocatalysis is an advanced oxidation processes (other AOPs: homogeneous photocatalysis, photolysis, Gamma-radiolysis) [12]. By means of heterogeneous photocatalysis, the goal is to break down different pollutants into less polluting substances [13]. In the case of heterogeneous photocatalysis, the photocatalyst can be excited with photons. When irradiated, the photocatalyst with photons of different energies, show photooxidative properties. Electron-hole pairs are created by electrons moving from the valance band to the conduction band [14]. This charge separation can promote redox reactions on the surface of the catalyst, whereupon reactive oxygen species could generate,

e.g., hydroxyl radical, H_2O_2 , peroxide radicals, hydroxyl anion, and superoxide anion [15]. Photocatalysts can usually be effectively excited with UV light, but the excitability can be increased by modifying the catalyst. One option is to reduce the band gap (excitation with visible light), while another option is to increase the recombination time (more reactive radicals are produced). We have three useful ways for modification: doping is when the crystalline structure is modified, decoration is when the surface of the photocatalyst is modified (e.g., metal deposition) and morphological modifications [16–18].

Doping photocatalysts with various elements (e.g., C, S, N, Ag, Cu) can reduce the bandgap energy, and, therefore, the photocatalyst could be activated with visible light as well and the dopant can act as an electron trap, which slows down the recombination of the electron-hole pairs, which also favors photocatalytic activity [16]. It has been proven that modifying TiO_2 with transition metals via different methods can help enhance photocatalytic efficiency under visible light. Some transition metals or transition metal oxides (Ag, Cu, CuO) have a plasmonic effect on the surface of the catalyst, which also increases the recombination time [18]. In the case of morphological modification, generally, the shape and porosity are modified [17].

In this work, we modified the SrTiO_3 photocatalyst with different amounts of plasmonic CuO_x nanoparticles by a reduction method, and the surface CuO_x content was optimized. Structure characterization methods were applied to prove the success of the photocatalyst preparation. Next, we determined the photocatalytic activity for all the prepared photocatalysts under UV illumination following the degradation of the phenol test molecule. The results showed that the modified SrTiO_3 had higher photocatalytic activity than pure SrTiO_3 .

2. Results and Discussion

2.1. Characterization

The crystal phase of the obtained photocatalyst was determined by XRD measurements. The characteristic reflection peaks of the modified and initial samples were located at the same 2Θ angle values and the ratio of the peaks was also similar, so the crystal lattice was not changed after the copper modification (Figure 1). The peaks belonged to the SrTiO_3 ((100), (110), (111), (200), (210), (211), (220), (300), (310) [19]). The XRD pattern for SrTiO_3 was assigned by the help of the SrTiO_3 JCPDS card (35–0734). Table 1 also contains the primary crystallite (not particle) sizes, calculated according to the Scherrer equation. The increase in the particle size also indicated the successful deposition of CuO_x .

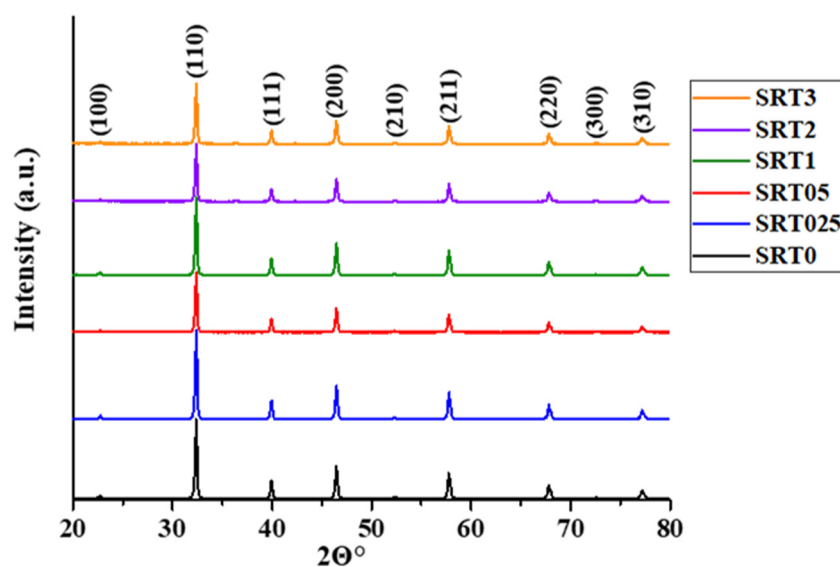
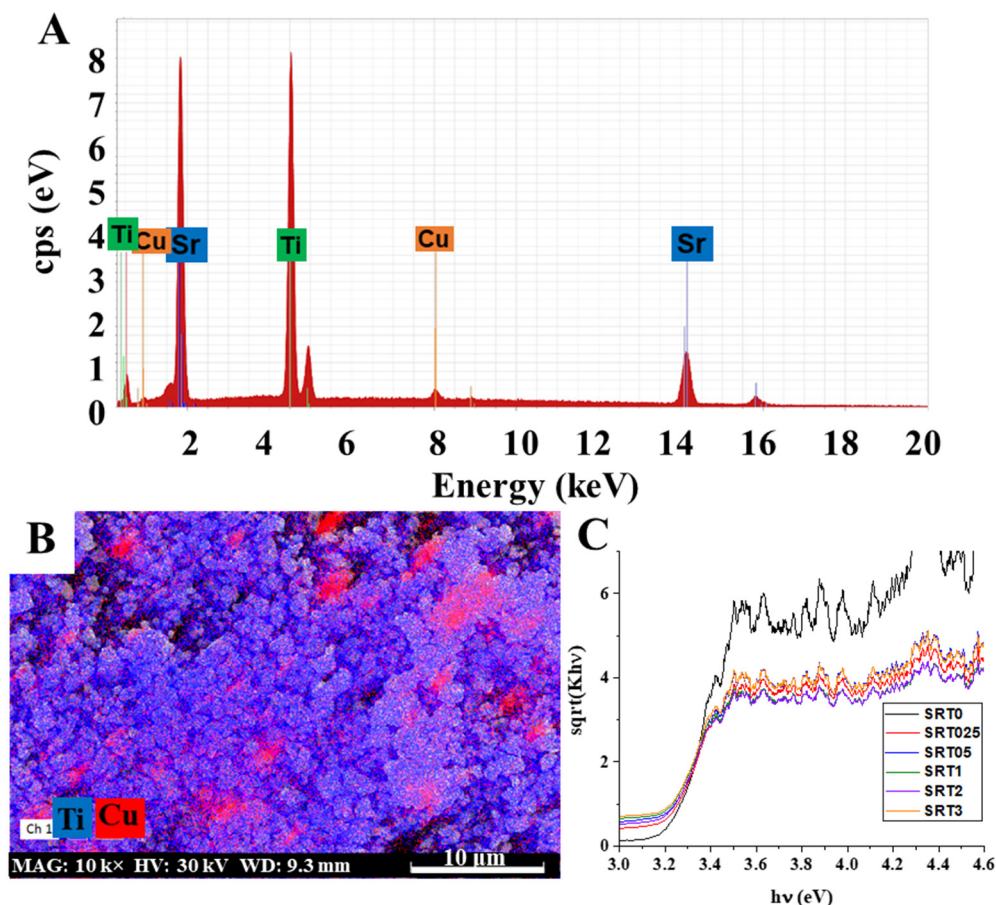


Figure 1. XRD patterns of SrTiO_3 and copper modified SrTiO_3 samples (SRTX).

Table 1. Nominal and measured Cu contents, specific surface area values and the primer crystallite size of the synthesized catalysts.

Catalyst Name	Nominal Cu-Content (wt.%)	Specific Surface Area (m ² /g)	Measured Cu-Content (wt.%)	Primary Crystallite Size (nm)	E _g (eV)
SRT0	0.00	2.06	0.00	5.30	3.22
SRT025	0.25	1.77	0.05	8.64	3.20
SRT05	0.50	2.07	0.81	9.10	3.19
SRT1	1.00	2.23	1.10	8.39	3.16
SRT2	2.00	2.11	2.77	7.86	3.17
SRT3	3.00	1.63	3.48	8.08	3.16

The presence of surface copper was also proved by EDX measurements. The EDX spectrum of the SRT1 sample, with 1 wt.% nominal Cu content, can be seen in Figure 2A. The characteristic lines of titanium, strontium and copper were clearly visible and it can also be seen that it did not contain significant amounts of other elements. By carrying out the measurements on the other samples (spectra are not presented), we could establish that the measured values did not always correspond to the nominal (theoretical, initial amount of copper) values, but followed a well-managed trend (Table 1). Moreover, we also carried out mapping measurements for the SRT1 sample with highest photocatalytic activity (photocatalytic activities see Section 2.2), in the resulting image we can see the presence of copper on the surface (Figure 2B). It can be seen that the coverage of CuO_x nanoparticles (red dots) was more or less uniform; however, local enrichment could also be observed in some cases. In the figure, the titanium is marked with blue. During the measurement, the titanium signal was set to a stronger contrast (this is why the image appears a little brighter), so that the CuO_x on the surface was more visible and more distinct.

**Figure 2.** Representative EDX spectrum of the CuO_x decorated SrTiO₃ catalyst with 1 wt.% Cu content

(SRT1) (A), the presence of CuO_x (red) on the surface of SrTiO_3 in the case of SRT1 sample EDX mapping (titanium marked with blue) (B) and Kubelka-Munk representation of SrTiO_3 and SRTX samples for bandgap energy determination (C).

Furthermore, the copper-modified samples were gray (gray-brown) in color, which also indicated the successful modification of the initial white strontium titanate. Therefore, the optical properties of the synthesized samples were also studied, by diffuse reflectance measurements (Figure 2C). The band gap energies (E_g) calculated by the Kubelka-Munk method [20] are presented in Table 1. As can be observed, the band gap values changed only slightly (from 3.16 to 3.22 eV), so this was not the primary reason for the increased photocatalytic activity (see later). However, the results showed that the wavelength dependence of the photocatalyst excitability was minimally improved by the copper deposition and the modified samples could be excited by lower energy photons, compared to initial SrTiO_3 .

TEM images of the initial SrTiO_3 (Figure 3A) and SRT1 (Figure 3B) with highest photocatalytic activity were also taken. The spherical CuO_x deposits located on the modified SrTiO_3 surfaces are marked with yellow arrows in Figure 3B. However, these $d = \sim 5\text{--}40$ nm surface nanoparticles were completely missing in the case of initial SrTiO_3 (SRT0, Figure 3A), and its surface was much smoother. This phenomenon was also confirmed by SEM mapping, where it was revealed that the coverage of CuO_x nanoparticles (red dots) was more or less uniform; however, local enrichment could also be observed in some cases (Figure 2B). The presence of CuO_x deposits on the SrTiO_3 particles increased the surface roughness, as well.

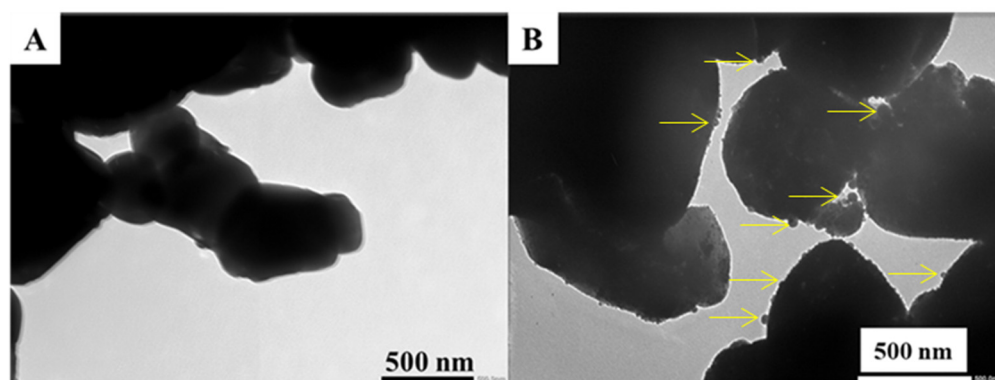


Figure 3. TEM image of the SRT0 (A) and SRT1 (B) sample.

Next, the specific surface area values of the synthesized photocatalyst were also measured and they are presented in Table 1. The SRT1 sample had the highest surface area ($2.23 \text{ m}^2/\text{g}$), which might also have contributed to the better photocatalytic activity. The porous structure of SrTiO_3 has been already reported on several times [21,22], so at lower Cu content, the copper deposit clogged the pores and, consequently, the specific surface area of the SRT025 sample was smaller ($1.77 \text{ m}^2/\text{g}$), compared to the SRT0 sample ($2.06 \text{ m}^2/\text{g}$). However, further increasing the copper content led to an increase in surface area, since no further copper deposit could enter the pores. As a result of the evolved Cu deposits (see Figure 3B), surface roughness developed, which had the largest specific surface area, and, then, the deposition of additional copper in small cavities “smooths” the surface, which was why the surface area decreased again.

The zeta potential change of the modified SrTiO_3 samples is illustrated in Figure 4. The initial SrTiO_3 was also measured for reference and its zeta potential was -40.15 ± 1.14 mV. Compared to the initial SrTiO_3 the copper modified samples had a slightly lower surface charge, ranging from -39.17 mV to -21.66 mV. The results indicated that the modification of the initial SrTiO_3 with CuO_x decreased the negative surface charge of the samples. According to the literature, the Zeta-potential of bare CuO is greater than -20 mV in

distilled water [23], and, thus, the change of the surface charge in the case of surface decorated catalysts is understandable, and consequently also proved the successful CuO_x deposition. The pH was around 9.15 for each sample and around 9 for the reference SrTiO_3 (SRT0). According to the literature, the change of the surface charge greatly influences the adsorption processes and the stability of the suspension [24].

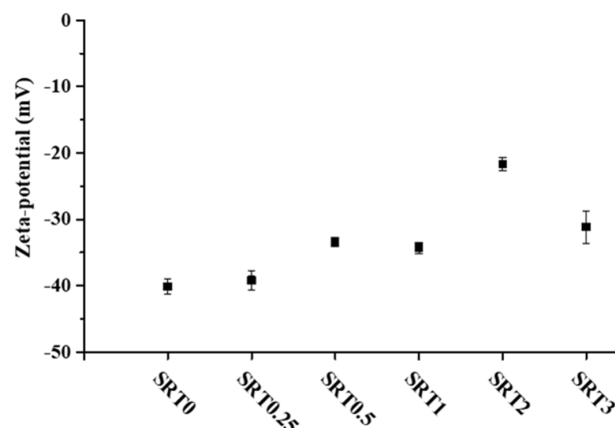


Figure 4. The zeta-potential values of 0.001 wt.% aqueous dispersion of the initial SrTiO_3 and SRTX samples (pH = ~9.15).

2.2. Photocatalytic Activity Measurements

Next, the photocatalytic activity of the synthesized catalyst was measured, under the same experimental conditions, and compared to the commercial (basic) SrTiO_3 (SRT0). Each surface modified sample had higher photocatalytic activity (~14.7–19.1% relative phenol decomposition) than the reference SrTiO_3 (~7% relative phenol decomposition, $0.690 \text{ mg}_{\text{phenol}}/\text{g}_{\text{cat}}$) and SRT1 showed the highest photocatalytic activity (19.1% relative phenol decomposition, $1.910 \text{ mg}_{\text{phenol}}/\text{g}_{\text{cat}}$). The results are summarised in Figure 5. (in Figure 5A the relative phenol decomposition curves can be seen, while in Figure 5B the degraded amount of phenol after 240 min irradiation is shown). As neither the band gap (Figure 2C) nor the surface charge (Figure 4) in this sample showed extreme values, better photocatalytic activity was sought elsewhere. Since the conversion of phenol takes place through hydroxyl radicals [25], so the amount of hydroxyl radical could be decisive in our system. The next section deals with this phenomenon. The photodegradation results showed that the optimum of the copper content was 1 wt.% for maximum photocatalytic activity, under certain conditions (UV excitation, 0.1 wt.% photocatalyst, and 10 mg/L initial concentration of phenol as pollutant).

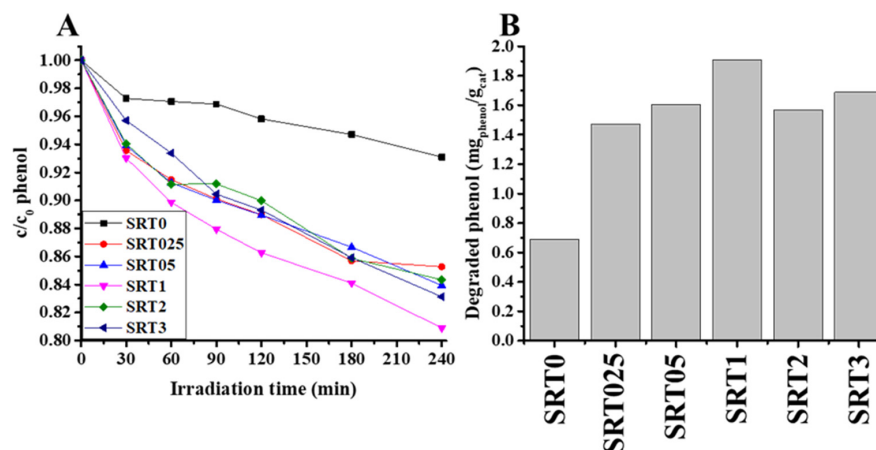


Figure 5. Photocatalytic activity of the SRTX photocatalysts and reference SrTiO_3 , run of decay curves (A) and the degraded specific amount of phenol ($\text{mg}_{\text{phenol}}/\text{g}_{\text{cat}}$) (B).

Next, the photocatalytic test was repeated in the case of the SRT1 sample with the highest photocatalytic activity to study the stability and reusability of the catalyst. Figure 6 shows the corresponding phenol photodegradation curves and the degraded specific amount of phenol ($\text{mg}_{\text{phenol}}/\text{g}_{\text{cat}}$) as a function of cycles. As shown in Figure 6, the catalyst did not exhibit any significant loss after three cycles of the degradation of phenol under the same conditions. The obtained degradation values were 19.1, 18.3 and 17% for the first, second and third cycles, respectively. The results confirmed that the obtained photocatalyst showed good stability and sustainability.

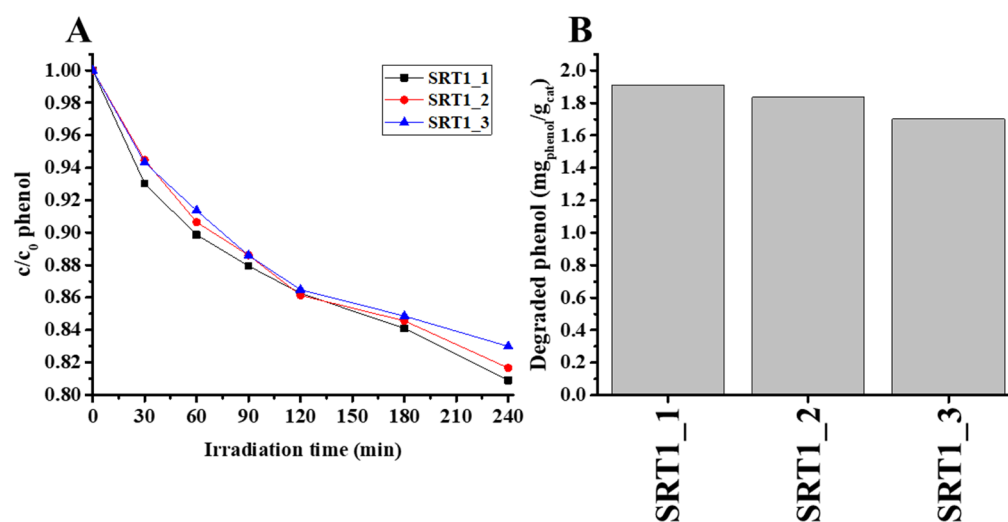


Figure 6. Photocatalytic activity of the SRT1 photocatalysts through 3 rounds, run of decay curves (A) and the degraded specific amount of phenol ($\text{mg}_{\text{phenol}}/\text{g}_{\text{cat}}$) (B).

2.3. Detection of Hydroxyl Radical

The 7-hydroxyumarin molecule is not detected without a catalyst, only the hydroxyl radicals formed during the photocatalytic process can produce 7-hydroxycoumarin [26]. The hydroxyl radical production capacity was measured with the same light source (Figure 7) that we applied during the photocatalytic tests.

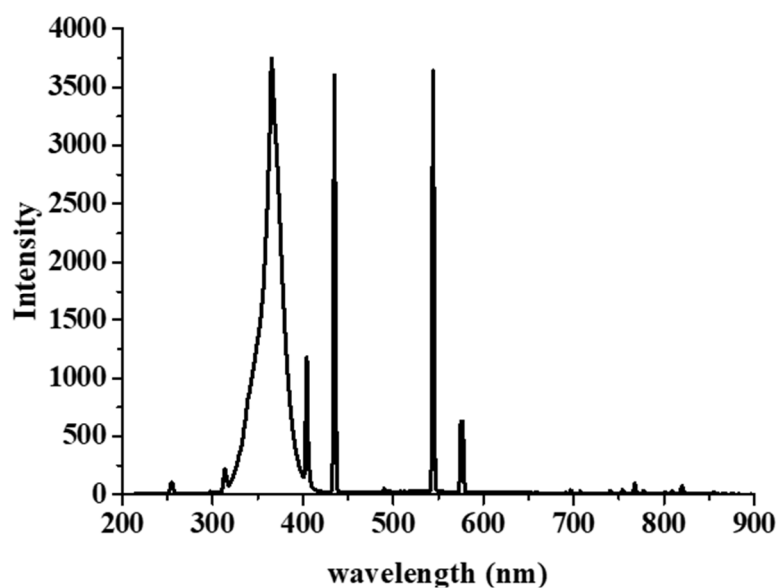


Figure 7. Emission spectrum of the used light source.

Figure 8 shows that the SRT1 had higher hydroxyl radical production capacity ($2.402 \times 10^{-6} \mu\text{mol} \times \text{L}^{-1} \times \text{s}^{-1}$) than the other SRT photocatalysts and the pure photocat-

alyst. SRT samples were better ability to produce hydroxyl radicals, because the surface of CuO_x has electron trapping ability (plasmonic effect) [27], so the charge separation takes longer, and, therefore, more water molecules could be oxidized on the hole side. The reaction rate constant was larger by an order of magnitude, thus proving that either more hole-electron pairs were formed and/or the recombination time was longer. The results showed that increasing the copper content did not linearly increase the hydroxyl radical production ability; the reason for this was probably the excessive copper coverage of the SrTiO_3 surface.

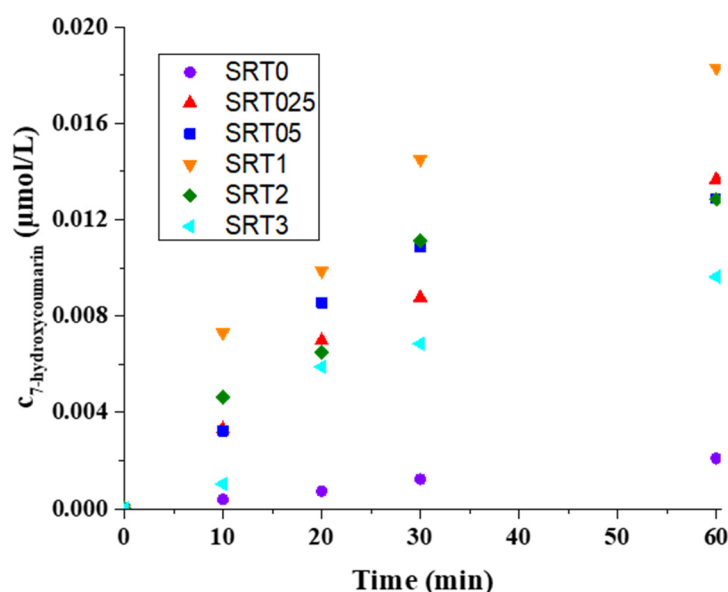


Figure 8. Production kinetics of 7-hydroxycoumarin from coumarin in the case of SrTiO_3 (SRT0) and in the case of the SRT samples.

3. Materials and Methods

3.1. Catalyst Preparation

Analytical grade chemicals were used for synthesis without further purification: SrTiO_3 (Alfa Aesar, Karlsruhe, Germany; >99%), $\text{CuSO}_4 \times 5 \text{H}_2\text{O}$ (Reanal Finomvegyszergyár, Budapest, Hungary; reagent grade), NaBH_4 (Molar Chemicals, Halásztelek, Hungary; 98.5%) and ultrapure Millipore Milli-Q water (Budapest, Hungary). CuO_x surface modified strontium titanate (SrTiO_3) samples were prepared using dissolved Cu^{2+} of a calculated amount and SrTiO_3 suspension. First, 10 mL 2.5 g/L Cu^{2+} solution (Cu ratio is 0.25 wt.%) was added to 100 mL 10 g/L SrTiO_3 suspension. After thorough mixing, an excess (20%) of reducing agent (NaBH_4) was used to successfully reduce all the copper, and, then, the mixture was stirred at 60 °C for 1 h. The samples were then calcinated for 3 h at 300 °C in airflow to oxidize the $\text{Cu}(\text{OH})_2$ on the surface. In the case of the other samples, the preparation procedure was the same, only the nominal Cu content (wt.%) was changed, the values are in the Table 1. SRT0 was the reference, commercial SrTiO_3 catalysts.

3.2. Characterization

The copper-modified SrTiO_3 samples' crystallinity was determined with X-ray diffraction measurements, which were carried out with a Philips X-ray diffractometer (PW 1830 generator, PW 1820 goniometer, $\text{CuK}\alpha$: $\lambda = 0.1542 \text{ nm}$, 40–50 kV, 30–40 mA) (Philips, Germany), from 20 to 80° (2θ), at room temperature.

For optical characterization, the diffuse reflectance spectra were recorded with UV-VIS USB4000 type (Ocean Optics Inc., Dunedin, FL, USA), diode array spectrophotometer. The spectrums were recorded from 200 to 850 nm wavelength. The bandgap values were determined using the Kubelka-Munk method [20].

The morphologies of the samples were analyzed, using a JEOL JEM-1400plus (JEOL Ltd., Tokyo, Japan) transmission electron microscope (TEM), operating with 120 kV accelerating voltage on Formvar foil covered 200 mesh copper grids.

The specific surface area values of the samples were measured by the BET method from N₂ adsorption isotherms (77 ± 0.5 K) by Micromeritics Gemini 2375 Surface Area Analyzer (Micromeritics, Norcross, GA, USA).

The electrophoretic mobility of the samples was also determined using a HORIBA SZ-100 Nanoparticle Analyzer (Horiba, Kyoto, Japan). During the measurements, a disposable carbon-coated electrode cell was used. From the measured data, the zeta-potential values were determined using the Smoluchowski model. The measured aqueous dispersions were prepared in 0.001 w/v% concentration from the copper-modified SrTiO₃ samples, as well as from the commercially available SrTiO₃ for comparison. The zeta-potential values provided useful information about the aqueous phase hydrodynamic stability as well [24].

Energy dispersive X-ray spectra were measured with Thermo Scientific Apreo C scanning electron microscope (Waltham, Massachusetts, USA) with Bruker XFlash 6-30 EDS detector (Billerica, MA, USA) (30 keV). We also performed the mapping measurements with this instrument.

3.3. Photocatalytic Activity Measurements

The photocatalytic efficiency of the SRTX (X denoted as nominal copper contents) samples was measured in aqueous suspension at room temperature. Phenol was used as model pollutant and the experiments were performed in an opened glass reactor. The used light source was fixed at 5 cm distance from the surface of continuously stirred (3500 rpm) 50 mL suspensions. The light source used during the photocatalytic tests emitted in the UV range (local λ_{\max} = 366 nm (Figure 8)). The photocatalyst concentration in the suspension was 0.1 wt.%, while the initial phenol concentration was 10 mg/L. The suspensions were irradiated for 90 min during the tests. The decreasing concentration of the model pollutant was followed by an Agilent 1290 Infinity II liquid chromatograph with UV detector (detection wavelength was 254 nm), the column was an InfinityLab Poroshell 120 ECsingle bondC18, while the mobile phase was 20/80 methanol/water with 1 mL/min flow rate. Before the irradiation, the suspensions were kept in the dark for 30 min to ensure adsorption equilibrium. The collected samples were centrifuged two times and filtered through 0.1 μ m Millex-VV PVDF filter before chromatographic analysis. With the best photocatalyst, we performed two rounds of reusability experiments in order to examine the stability of the catalyst, and the stability of the given catalyst could be deduced from the change in photocatalytic activity.

3.4. Detection of Hydroxyl Radical

The hydroxyl radicals were detectable by their reaction with coumarin (Figure 9) [26]. Coumarin reacts with the hydroxyl radical if it is present in the system and the result of the reaction is 7-hydroxycoumarin, a molecule which is detectable through its emission (λ_{\max} = 453 nm). The capacity of the hydroxyl radical production was measured for the initial SrTiO₃ and all SRTX samples. The experiments were preceded by the calibration of the spectrofluorometer (HORIBA Jobin Yvon Fluoromax-4) with 7-hydroxycoumarin, the concentration dependence was linear over the range used (1×10^{-8} mol/L– 5×10^{-6} mol/L), R₂ = 0.9999.

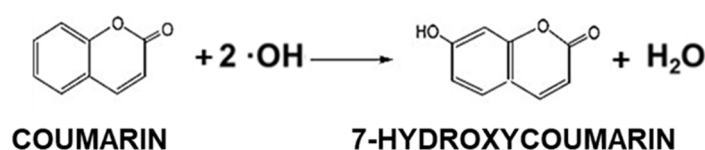


Figure 9. Hydroxyl radical reaction with coumarin resulted 7-hydroxycoumarin.

For measurements, the initial coumarin concentration was 1×10^{-4} mol/L, and the photocatalyst concentration was 0.1 wt.%. The UV light source was placed at 5 cm distance from the suspensions surface. The actual 7-hydroxycoumarin concentration change was determined by a Jasco FP-8500 spectrofluorometer. The excitation wavelength of 7-hydroxycoumarin was 345 nm, while the detection wavelength was 453 nm. Before the measurements, the samples were centrifuged two times to completely remove the dispersed photocatalyst particles.

4. Conclusions

Plasmonic strontium titanate-based photocatalyst, with varied surface copper content (CuO_x), having improved photocatalytic activity was synthesized. The successful modification of the photocatalyst surface was proven by XRD (increased the primary crystallite size from 5.3 nm to ~8.5 nm), diffuse reflectance and zeta-potential measurements. EDX, SEM-mapping and TEM measurements proved the presence of copper nanoparticles ($d = \sim 5\text{--}40$ nm) on the surface of SrTiO_3 particles ($d = \sim 500\text{--}1500$ nm). According to the BET measurements, the SRT1 sample had the largest specific surface area ($2.23 \text{ m}^2/\text{g}$), which probably also contributed to its increase in photocatalytic activity. Through the breakdown of the phenol test molecule, we established that the SRT1 sample had the highest photocatalytic activity ($1.910 \text{ mg}_{\text{phenol}}/\text{g}_{\text{cat}}$), so the optimal copper content was around 1 wt.%. According to the reusability tests, the photocatalytic activity decreased minimally. When examining the origin of 7-hydroxycoumarin, which is related to the amount of hydroxyl radical produced, we found that the reason for the increase in photocatalytic activity could be explained by the increased amount of hydroxyl radical. The 7-hydroxycoumarins concentrations were 2.8×10^{-7} and $2.4 \times 10^{-6} \mu\text{mol} \times \text{L}^{-1} \times \text{s}^{-1}$, in the case of STR0 and STR1, respectively. An increase in the amount of hydroxyl radicals indicated that more surface adsorbed water molecules were oxidized, which was due to the plasmonic effect of CuO_x , which increases the charge recombination time, i.e., water molecules have more time to oxidize into hydroxyl radicals. Consequently, at optimal Cu content (1%) the plasmonic enhancement of the surface CuO_x particles decreased the electron-hole recombination rate. However, further increasing the Cu content meant the particles might block the active sites of the catalyst.

Author Contributions: Á.Á.: Conceptualization, Methodology, Investigation, Original draft, Á.B.: Investigation, Š.N.: Investigation, I.D.: Writing—review & editing, L.J.: Funding acquisition, Writing—review & editing. All authors have read and agreed to the published version of the manuscript.

Funding: The authors are very thankful for the financial support from the National Research, Development and Innovation Office (GINOP-1.1.2-PIACI-KFI-2021-00193) and for the Hungarian Scientific Research Fund (OTKA) FK 142437. This paper was also supported by the UNKP-22-5 New National Excellence Program of the Ministry for Innovation and Technology from the National Research, Development and Innovation Fund and by the János Bolyai Research Scholarship of the Hungarian Academy of Sciences. The authors are very thankful for the financial support received from UAB “Kai reikia” via the project “Development of a universal titanium dioxide coating with long-term disinfecting properties” No. 01.2.1-LVPA-T-858-01-0056 which is partially funded by the European Union.

Institutional Review Board Statement: Not applicable.

Informed Consent Statement: Not applicable.

Data Availability Statement: Not applicable.

Conflicts of Interest: The authors declare that they have no known competing financial interests or personal relationships that could have appeared to influence the work reported in this paper.

References

1. Rodriguez, C.; Di Cara, A.; Renaud, F.N.R.; Freney, J.; Horvais, N.; Borel, R.; Puzenat, E.; Guillard, C. Antibacterial Effects of Photocatalytic Textiles for Footwear Application. *Catal. Today* **2014**, *230*, 41–46. [[CrossRef](#)]
2. Mills, A.; Davies, R.H.; Worsley, D. Water Purification by Semiconductor Photocatalysis. *Chem. Soc. Rev.* **1993**, *22*, 417–425. [[CrossRef](#)]
3. Ali, H.; Zaman, S.; Majeed, I.; Kanodarwala, F.K.; Nadeem, M.A.; Stride, J.A.; Nadeem, M.A. Porous Carbon/RGO Composite: An Ideal Support Material of Highly Efficient Palladium Electrocatalysts for the Formic Acid Oxidation Reaction. *ChemElectroChem* **2017**, *4*, 3126–3133. [[CrossRef](#)]
4. Zhou, Y.; Wang, Z.; Huang, L.; Zaman, S.; Lei, K.; Yue, T.; Li, Z.; You, B.; Xia, B.Y.; Zhou, Y.; et al. Engineering 2D Photocatalysts toward Carbon Dioxide Reduction. *Adv. Energy Mater.* **2021**, *11*, 2003159. [[CrossRef](#)]
5. Noureen, L.; Xie, Z.; Gao, Y.; Li, M.; Hussain, M.; Wang, K.; Zhang, L.; Zhu, J. Multifunctional Ag₃PO₄-RGO-Coated Textiles for Clean Water Production by Solar-Driven Evaporation, Photocatalysis, and Disinfection. *ACS Appl. Mater. Interfaces* **2020**, *12*, 6343–6350. [[CrossRef](#)] [[PubMed](#)]
6. Noureen, L.; Xie, Z.; Hussain, M.; Li, M.; Lyu, Q.; Wang, K.; Zhang, L.; Zhu, J. BiVO₄ and Reduced Graphene Oxide Composite Hydrogels for Solar-Driven Steam Generation and Decontamination of Polluted Water. *Sol. Energy Mater. Sol. Cells* **2021**, *222*, 110952. [[CrossRef](#)]
7. Solís, R.R.; Bedia, J.; Rodríguez, J.J.; Belver, C. A Review on Alkaline Earth Metal Titanates for Applications in Photocatalytic Water Purification. *Chem. Eng. J.* **2021**, *409*, 128110. [[CrossRef](#)]
8. Hashimoto, K.; Irie, H.; Fujishima, A. TiO₂ Photocatalysis: A Historical Overview and Future Prospects. *Jpn. J. Appl. Phys. Part 1 Regul. Pap. Short Notes Rev. Pap.* **2005**, *44*, 8269–8285. [[CrossRef](#)]
9. Tenzin, T.; Yashas, S.R.; Anilkumar, K.M.; Shivaraju, H.P. UV-LED Driven Photodegradation of Organic Dye and Antibiotic Using Strontium Titanate Nanostructures. *J. Mater. Sci. Mater. Electron.* **2021**, *32*, 21093–21105. [[CrossRef](#)]
10. Jiang, J.; Kato, K.; Fujimori, H.; Yamakata, A.; Sakata, Y. Investigation on the Highly Active SrTiO₃ Photocatalyst toward Overall H₂O Splitting by Doping Na Ion. *J. Catal.* **2020**, *390*, 81–89. [[CrossRef](#)]
11. Phoon, B.L.; Lai, C.W.; Juan, J.C.; Show, P.L.; Pan, G.T. Recent Developments of Strontium Titanate for Photocatalytic Water Splitting Application. *Int. J. Hydrogen Energy* **2019**, *44*, 14316–14340. [[CrossRef](#)]
12. Farré, M.J.; Franch, M.I.; Malato, S.; Ayllón, J.A.; Peral, J.; Doménech, X. Degradation of Some Biorecalcitrant Pesticides by Homogeneous and Heterogeneous Photocatalytic Ozonation. *Chemosphere* **2005**, *58*, 1127–1133. [[CrossRef](#)] [[PubMed](#)]
13. Margot, J.; Rossi, L.; Barry, D.A.; Holliger, C. A Review of the Fate of Micropollutants in Wastewater Treatment Plants. *Wiley Interdiscip. Rev. Water* **2015**, *2*, 457–487. [[CrossRef](#)]
14. Reydellet, L.-H.; Roche, P.; Glattli, D.C.; Etienne, B.; Jin, Y. Quantum Partition Noise of Photon-Created Electron-Hole Pairs. *Phys. Rev. Lett.* **2003**, *90*, 176803. [[CrossRef](#)]
15. Vieira, Y.; Leichtweis, J.; Foletto, E.L.; Silvestri, S. Reactive Oxygen Species-Induced Heterogeneous Photocatalytic Degradation of Organic Pollutant Rhodamine B by Copper and Zinc Aluminate Spinels. *J. Chem. Technol. Biotechnol.* **2020**, *95*, 791–797. [[CrossRef](#)]
16. Cravanzola, S.; Cesano, F.; Gaziano, F.; Scarano, D. Sulfur-Doped TiO₂: Structure and Surface Properties. *Catalysts* **2017**, *7*, 214. [[CrossRef](#)]
17. Gyulavári, T.; Dusnoki, D.; Márta, V.; Yadav, M.; Abedi, M.; Sápi, A.; Kukovecz, Á.; Kónya, Z.; Pap, Z. Dependence of Photocatalytic Activity on the Morphology of Strontium Titanates. *Catalysts* **2022**, *12*, 523. [[CrossRef](#)]
18. Sakthivel, S.; Shankar, M.V.; Palanichamy, M.; Arabindoo, B.; Bahnemann, D.W.; Murugesan, V. Enhancement of Photocatalytic Activity by Metal Deposition: Characterisation and Photonic Efficiency of Pt, Au and Pd Deposited on TiO₂ Catalyst. *Water Res.* **2004**, *38*, 3001–3008. [[CrossRef](#)]
19. Da Silva, L.F.; Avansi, W.; Moreira, M.L.; Mesquita, A.; Maia, L.J.Q.; Andrés, J.; Longo, E.; Mastelaro, V.R. Relationship between Crystal Shape, Photoluminescence, and Local Structure in SrTiO₃ Synthesized by Microwave-Assisted Hydrothermal Method. *J. Nanomater.* **2012**, *2012*, 890397. [[CrossRef](#)]
20. Gillespie, J.B.; Lindberg, J.D.; Laude, L.S. Kubelka-Munk Optical Coefficients for a Barium Sulfate White Reflectance Standard. *Appl. Opt.* **1975**, *14*, 807–809. [[CrossRef](#)]
21. Dong, W.; Li, X.; Yu, J.; Guo, W.; Li, B.; Tan, L.; Li, C.; Shi, J.; Wang, G. Porous SrTiO₃ Spheres with Enhanced Photocatalytic Performance. *Mater. Lett.* **2012**, *67*, 131–134. [[CrossRef](#)]
22. Wang, Y.; Xu, H.; Wang, X.; Zhang, X.; Jia, H.; Zhang, L.; Qiu, J. A General Approach to Porous Crystalline TiO₂, SrTiO₃, and BaTiO₃ Spheres. *J. Phys. Chem. B* **2006**, *110*, 13835–13840. [[CrossRef](#)]
23. Huang, C.C.; Lo, S.L.; Tsai, S.M.; Lien, H.L. Catalytic Hydrodechlorination of 1,2-Dichloroethane Using Copper Nanoparticles under Reduction Conditions of Sodium Borohydride. *J. Environ. Monit.* **2011**, *13*, 2406–2412. [[CrossRef](#)] [[PubMed](#)]
24. Gallardo, V.; Morales, M.E.; Ruiz, M.A.; Delgado, A.V. An Experimental Investigation of the Stability of Ethylcellulose Latex: Correlation between Zeta Potential and Sedimentation. *Eur. J. Pharm. Sci.* **2005**, *26*, 170–175. [[CrossRef](#)] [[PubMed](#)]
25. Jayathilaka, P.B.; Pathiraja, G.C.; Bandara, A.; Subasinghe, N.D.; Nanayakkara, N. Theoretical Study of Phenol and Hydroxyl Radical Reaction Mechanism in Aqueous Medium by the DFT/B3LYP/6-31+G(d,p)/CPCM Model. *Can. J. Chem.* **2014**, *92*, 809–813. [[CrossRef](#)]

-
26. Maier, A.C.; Iglebaek, E.H.; Jonsson, M. Confirming the Formation of Hydroxyl Radicals in the Catalytic Decomposition of H₂O₂ on Metal Oxides Using Coumarin as a Probe. *ChemCatChem* **2019**, *11*, 5435–5438. [[CrossRef](#)]
 27. Chiang, K.; Amal, R.; Tran, T. Photocatalytic Degradation of Cyanide Using Titanium Dioxide Modified with Copper Oxide. *Adv. Environ. Res.* **2002**, *6*, 471–485. [[CrossRef](#)]